A DFT Study of Two Diiron (II) Synthetic Model Compounds and Their Diiron(III) Peroxide Oxygenation Products

R. C. BINNING JR.,[1] DANIEL E. BACELO[1,2]

[1]*School of Sciences and Technology, Universidad Metropolitana, P. O. Box 21150, San Juan, PR 00928-1150, USA*

[2]*Dpto. de Química, FCN, Universidad Nacional de la Patagonia San Juan Bosco, Km. 4, (9000) Comodoro Rivadavia, Chubut, Argentina*

Received 25 March 2009; accepted 4 May 2009
Published online 29 July 2009 in Wiley InterScience (www.interscience.wiley.com).
DOI 10.1002/qua.22350

ABSTRACT: Unrestricted density functional theory calculations have been conducted on two diiron(II) synthetic model compounds. Calculations employed the BPW91 and BOP density functionals with both high-spin and broken symmetry low-spin representations of weakly coupled high-spin irons. Comparison of the calculated and crystallographic structures is made, and good agreement is found with both spin representations. Raman spectral data are available for the diiron(III) product of the reaction with O_2 to form a bridged peroxide. Calculated harmonic frequencies confirm the experimental assignments. Small geometry differences between the high spin and broken symmetry results are seen in bond lengths, angles, Raman frequencies, and spin densities associated with oxo and peroxo bridges in the diiron(III) oxidation products.
 Int J Quantum Chem 109: 3533–3540, 2009

Key words: broken symmetry; ferromagnetic coupling; antiferromagnetic coupling; weak exchange coupling; diiron center; density functional theory

Correspondence to: R. C. Binning; e-mail: binningrc@yahoo.com or D. E. Bacelo; e-mail: um_dbacelo@suagm.edu
Contract grant sponsor: National Science Foundation.
Contract grant number: MCB-0641269.

Introduction

Diiron centers occur widely in proteins [1, 2]. In enzymes, they serve to activate O_2 for a variety of redox processes; in hemerythrin [3], the diiron center binds oxygen for transport, and in the iron-storage protein ferritin, the diiron center is a substrate that is oxidized and transported to a storage site in the center of the protein [4, 5].

In the majority of protein diiron(II) and (III) centers, each iron is high spin (HS). The two ions are typically bridged by common ligands and weakly coupled. They may be either aligned or opposed to yield overall a ferromagnetically coupled HS or an antiferromagnetically coupled low-spin state, and theoretical methods applied to these structures must represent both.

Density functional theory (DFT) is the most practical all-electron theoretical approach for systems as large as protein fragments with diiron centers, and nearly all theoretical work on protein diiron centers is DFT based. DFT in the Kohn–Sham formulation [6] is by long-established convention a single-configuration method [7, 8]. Although the high-spin state presents no fundamental problem, a singlet arising from two spin-opposed high-spin atoms is inherently multiconfigurational. Two approaches are taken in applying DFT to antiferromagnetically coupled dimetallics.

Although the spins are opposed, the center may simply be treated as high spin. This representation is theoretically sound, and whatever errors in optimized geometries that arise from the incorrect electronic state are assumed small because the ions interact weakly. Good energetic and geometric results have been obtained with the approximation [9, 10].

An alternative to HS is the "broken symmetry," [11, 12] low-spin (BSLS) approach in which the DFT calculation is carried out by constructing opposed spin densities on the metal ions. The result is not a pure spin state, but the energies of the pure-spin states can be recovered if the energy of one, and the broken symmetry energy, are known. The HS-BSLS energy difference is $E_{HS} - E_{BS} = -4JS_1S_2$ in the Heisenberg weak-coupling approximation, where S_1 and S_2 are the spins on the two centers, and J is the exchange coupling constant [12]. Broken symmetry calculations have the variational flexibility to represent charge distributions accurately, and they have found extensive use with diiron and other metalloenzymes [13–15].

Molecular geometries calculated in the HS and BSLS approaches exhibit some differences [16], but there have been few direct comparisons to experimental structures of molecular geometries optimized with both spin representations. The majority of all-electron calculations must truncate the protein environments around diiron centers, and consequently it is difficult to positively identify whether the sources of discrepancies arise from computational representation or from truncation effects. However, synthetic model compounds [17, 18] do offer a means of directly comparing theoretical results. Model compounds are designed to incorporate protein functionality in a molecule of modest size. The compounds are typically well characterized crystallographically and spectroscopically and potentially provide a number of points of comparison.

A recent study of the geometries of three antiferromagnetically coupled low-spin diiron(III) model compounds examined the geometric differences associated with the HS and BSLS representations [15]. In both HS and BSLS calculations, the basic arrangements of ligands around the metal ions were found to be satisfactorily represented. Differences associated with the two approaches were minor and confined primarily to the bridging ligands.

This study slightly broadens the previous study of diiron(III) centers. It focuses on two diiron(II) model compounds, one of which is presumed to be high spin. Both diiron(II) model compounds were synthesized to mimic reactions with O_2 to form diiron(III) peroxides. The structures of the iron(III) complexes were not crystallographically determined, but both were subjected to resonance Raman spectroscopic analysis, and therefore the DFT calculations were also done to optimize the structures and obtain the harmonic vibrational spectra.

Compound **1** (see Fig. 1), $[Fe_2(\mu\text{-}OH)_2(6\text{-}Me_3\text{-}TPA)_2](ClO_4)_2$, where 6-$Me_3$-TPA is tris(6-methyl-2-pyridylmethyl)amine, was synthesized by Que and coworkers [19] to study the diiron center of the R2 subunit of ribonucleotide reductase (RNR). The electronic state was not conclusively determined, but it was found to give an electron spin resonance signal consistent with a high-spin complex and consistent with the state of the diiron(II) center of RNR. DFT geometry optimizations were done on the dication.

Compound **2** (see Fig. 2), is $[Fe_2(Me_4\text{-tpdp})(C_6H_5COO)(H_2O)](BF_4)_2$, where Me_4-tpdp is N, N, N′, N′-tetrakis{(6-methyl-2-pyridyl)methyl}-1,3-diaminopropan-2-olate. It was synthesized and char-

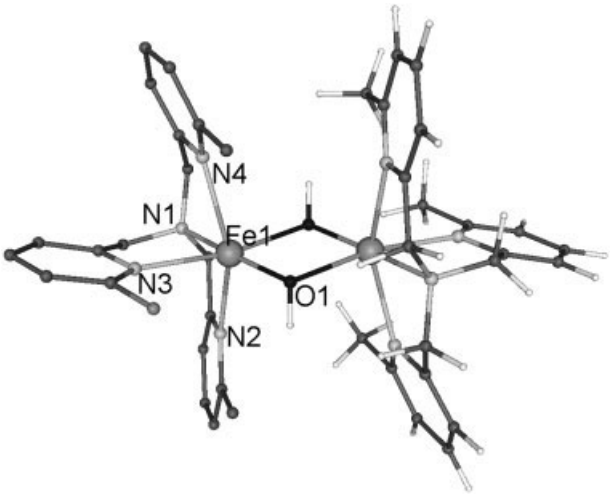

FIGURE 1. BPW91/DNP broken symmetry optimized structure of Compound **1**. Oxygen atoms are black, carbons dark gray, nitrogens light gray, and hydrogens white. Iron atoms are gray and larger. Hydrogens are omitted from half the molecule to facilitate viewing.

acterized by Hayashi et al. [20] The low-spin state composed of antiferromagnetically coupled high-spin ions was established from the curve of the temperature dependence of the magnetic susceptibility [21]. The exchange coupling constant was measured as $J = -8.6\ cm^{-1}$, indicating very weak coupling of the centers. Mössbauer parameters were also noted to be appropriate for high-spin iron(II) complexes. Geometry optimizations were performed by removing the two BF_4^- ions from the crystal structure and treating the dication. The ligands of both model compounds incorporated bulky groups intended to affect reactivity, and these provide a significant challenge to accurate modeling of the geometries.

Methods

Energies were obtained in spin-unrestricted density functional theory calculations. The BPW91 and BOP generalized gradient approximation (GGA) functionals were employed. BPW91 and BOP both employ Becke's [22] exchange functional. BPW91 uses the gradient-corrected correlation functional of Perdew et al. [23], while BOP uses the one-parameter progressive correlation functional of Tsuneda et al. [24]. In employing two closely related functionals, some assessment of the size of error attributable to variation in the nature of the density functional may be made and compared to the differences seen between the two spin representations employed. Calculations were carried out with the DMol^3 program, using basis sets of double numerical plus polarization (DNP) quality [25, 26].

Results and Discussion

The structures of diiron(II) Compounds **1** and **2** were optimized in DFT calculations in the HS and BSLS spin density representations. The BPW91/DNP optimized geometry of **1** is displayed in Figure 1, and a superposition of the structure of Figure 1 with the experimental structure [19] is shown in Figure 3. Similarly, the optimized structure of **2** is displayed in Figure 2, and superposition on the experimental structure [20] is shown in Figure 4. Tables I and II, respectively, contain calculated and experimental bond lengths and angles that characterize the ligand environments of **1** and **2**. Calculated total energies are shown in Table III. Each optimization resulted in bond lengths or angles that deviated from the corresponding crystallographic values, but each qualitatively represented the structures of the model compounds correctly; neither the bonds were broken, nor were the conformational changes introduced in the optimizations. The DFT calculations found Compound **1** to be a low-spin complex, whereas experimentally it was found to

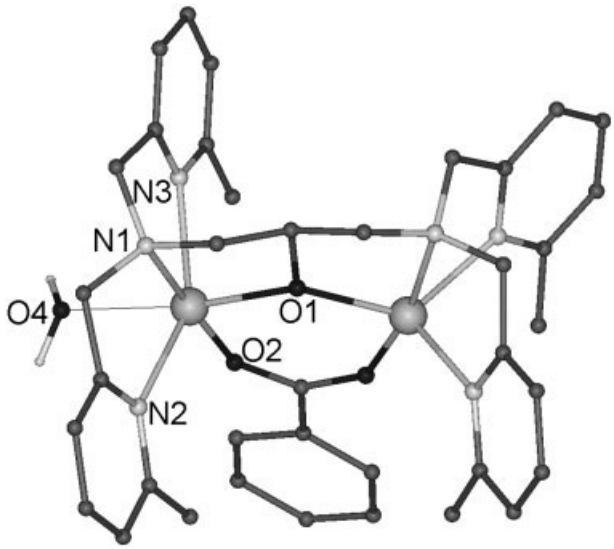

FIGURE 2. BPW91/DNP broken symmetry optimized structure of Compound **2**. Atom numbers are referred to throughout the text. Hydrogens have been omitted.

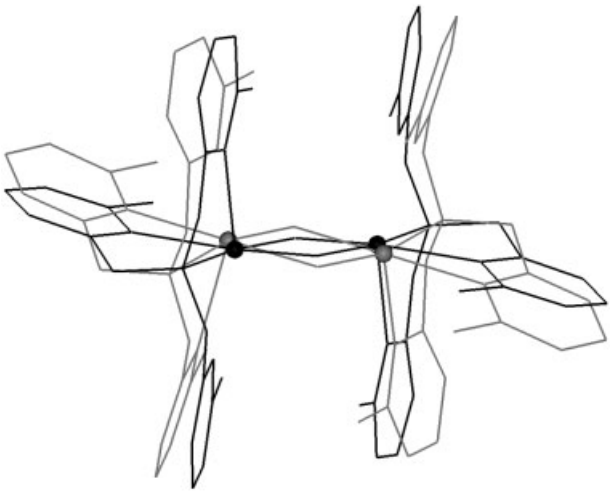

FIGURE 3. Superposition of the calculated structure of **1** from Figure 1 (gray), shown in line representation with hydrogen atoms omitted, and the experimental structure [19] (black).

have unpaired electrons [19]. This may be an example of the tendency of GGA functionals to favor low-over high-spin states [27, 28].

The calculated geometries of Compounds **1** and **2** (Tables I and II, respectively) are immediately seen to betray little variation attributable to spin representation. HS and BSLS bond angles and Fe—N bond lengths in general agree closely. Fe—O bond lengths do show greater discrepancies, but there is less difference between corresponding HS and BSLS lengths than between either of these and experiment, or between corresponding BPW91 and BOP results.

In a previous study of diiron(III) complexes [15], both BPW91 and BOP calculations were found to overestimate Fe-ligand bond lengths in general, and the same tendency is to be seen in the calculated bond lengths of **1** and **2**. Overestimation is somewhat greater with BOP than with BPW91 so the latter functional yields the more accurate geometries. Bond angles calculated with both functionals generally agree well with experiment, indicating that the spatial arrangement of the ligands is captured correctly. The Fe—O bonds in the central diamond of **1** are alternately unusually long and short, and this is correctly described in the calculated structures. The largest errors to be noted in Figures 3 and 4 are the displacements of the bulky pyridyl groups, but these are peripheral to the primary ligand attachments. The HS and BSLS geometry differences are small, even in the bonds to atoms that bridge the two centers.

The very weak coupling between the iron centers may explain the agreement between the HS and BSLS geometries. The Heisenberg coupling constant for **1** was not measured, but the BPW91 calculated $J = -7.1\ \mathrm{cm}^{-1}$, and the BOP value of $-1.2\ \mathrm{cm}^{-1}$ indicate weak interaction. In Compound **2**, the measured $J = -8.6\ \mathrm{cm}^{-1}$. The BPW91 calculated $J = -9.2\ \mathrm{cm}^{-1}$, and the BOP $J = -9.3\ \mathrm{cm}^{-1}$ agree fortuitously well with experiment and are quite small.

Compounds **1** and **2** were both synthesized to simulate the formation of diiron(III) bridging peroxide intermediates in the reactions of the diiron(II) complexes with O_2. Consequently, the reactions of both with O_2 were carried out at low temperature, and the existence of the peroxo bridge in each was diagnosed through its resonance Raman spectrum [19, 20]. DFT geometry optimizations of the diiron(III) peroxides were also carried out, and the BPW91/DNP HS and BSLS harmonic vibrational spectra were obtained. The peroxide resulting from reaction of **1** with O_2 is Compound **3**, and the optimized structure is depicted in Figure 5. Figure 6 depicts Compound **4**, the peroxide product of **2** and O_2. Table III also contains an entry for Compound **5**. Because the addition of O_2 to **2** displaces a water

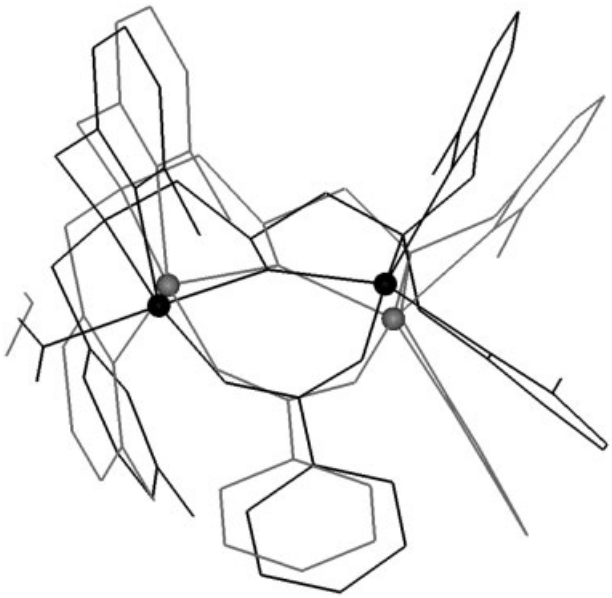

FIGURE 4. Superposition of the calculated structure of **2** from Figure 2 (gray) and the experimental structure [20] (black).

TABLE I

Compound 1— crystallographic and calculated distances (Å) and bond angles (°).

	Expt.	HS		BS-LS	
	[19]	BPW91	BOP	BPW91	BOP
Fe–Fe	3.187	3.257	3.313	3.278	3.346
Fe–O1	1.973	2.002	2.010	1.993	1.999
Fe–O1*	2.168	2.218	2.254	2.238	2.283
Fe–N1	2.222	2.252	2.364	2.293	2.272
Fe–N2	2.285	2.427	2.563	2.422	2.354
Fe–N3	2.326	2.297	2.273	2.250	2.426
Fe–N4	2.290	2.352	2.438	2.347	2.553
Fe–O1–Fe	100.6	100.9	101.8	101.4	102.6
N1–Fe–O1	169.0	167.2	167.4	166.9	167.0
N2–Fe–O1	104.6	100.8	100.9	101.0	101.3
N3–Fe–O1	112.5	113.0	112.6	113.2	113.1
N4–Fe–O1	105.0	111.6	113.4	111.3	112.8
N1–Fe–N2	73.7	72.4	71.2	72.4	71.2
N3–Fe–N4	83.3	80.5	80.2	80.8	80.6

molecule, it is necessary to know the energy of **2** without the water molecule to calculate the binding energy of O_2. Compound **5** is that dehydrated di-iron(II) complex.

The experimental spectrum of **3** was found to consist of bands at 462 cm^{-1}, 531 cm^{-1}, and 848 cm^{-1} [19]. The bands involving motion of the peroxo oxygen atoms were distinguished from the complex arising from the other oxygen ligands by isotope shift. The three were assigned, respectively, to a symmetric Fe—O stretch, an asymmetric Fe—O stretch and the O—O stretch. Harmonic analysis of the region near the BPW91/DNP HS minimum energy geometry finds Fe—O stretches at 357 cm^{-1} and 447 cm^{-1}, with the O—O stretch at 960 cm^{-1}. The corresponding modes in the BSLS representation lie at 469 cm^{-1} and 552 cm^{-1}, while the O—O stretching frequency is 876 cm^{-1}. Both sets of cal-

TABLE II

Compound 2— experimental and calculated distances (Å) and bond angles (°).

	Expt.	HS		BS-LS	
	[20]	BPW91	BOP	BPW91	BOP
Fe–Fe	3.684	3.780	3.811	3.747	3.782
Fe1–O1	2.060	2.082	2.116	2.058	2.099
Fe1–O2	2.066	2.000	2.016	2.010	2.024
Fe1–O4	2.142	2.344	2.421	2.353	2.435
Fe1–N1	2.200	2.232	2.264	2.228	2.263
Fe1–N2	2.287	2.344	2.410	2.338	2.406
Fe1–N3	2.337	2.321	2.382	2.329	2.385
Fe2–N4	2.195	2.249	2.283	2.248	2.282
Fe2–N5	2.202	2.209	2.273	2.210	2.269
Fe2–N6	2.175	2.216	2.270	2.220	2.278
Fe–O–Fe	131.2	131.5	130.7	131.3	130.4
O2–Fe1–N2	105.3	103.7	104.2	103.6	104.3
N1–Fe1–N2	76.7	75.8	75.3	76.0	75.3
O3–Fe2–N5	96.5	105.8	105.6	105.3	105.2
N4–Fe2–N5	74.9	75.8	77.2	76.9	75.5

TABLE III

Calculated–E (hartree)[a] of optimized compounds.

Compound	HS		BSLS	
	BPW91	BOP	BPW91	BOP
1	4747.17425	4746.14557	4747.17477	4746.14566
2	4632.08328	4631.12915	4632.08433	4631.13021
3	4897.55578	4896.51302	4897.67098	4896.52783
4	4706.00750	4705.04913	4706.02164	4705.06141
5	4555.62087	4554.68001	4555.63570	4554.69519

[a] The BPW91/DNP calculated energies of $^3O_2$ and H_2O are, respectively, –150.38931 and –76.46022 a.u. The corresponding BOP/DNP energies are –150.37799 and –76.44975 a.u.

culations affirm the experimental assignments as arising from motions of atoms comprising the peroxide bridge.

The differences in the HS and BSLS calculated frequencies in **3** are foreshadowed by the charge density distributions and geometries. In the HS calculation, Fe—O bond lengths are 1.99 Å and 2.03 Å. The peroxide O—O distance is 1.36 Å. In the BSLS calculation, the Fe—O bond lengths are both 1.81 Å, with the O—O length 1.37 Å. These correspond roughly with the lower Fe—O and higher O—O frequencies found with HS. Examining the charge distributions by means of population analysis, the HS calculation places 0.5 electron spin on each peroxide oxygen, with the same polarization as found on the Fe ions. The BSLS calculation places smaller spin densities, 0.1 spin, on each oxygen. The BSLS calculation yields a slightly shorter, stronger Fe—O bond and a slightly longer, weaker O—O bond than the HS, and the calculated frequencies reflect these differences.

Four Raman frequencies were associated with the bridging peroxide in Compound **4** [20]. Low frequencies at 450 cm^{-1} and 486 cm^{-1} were assigned to Fe—O stretches. A higher frequency doublet at 891 cm^{-1} and 918 cm^{-1} was assigned to symmetric and asymmetric stretches of the peroxide moiety. The calculated HS harmonic frequencies for **4** are quite similar to those obtained for Compound **3** and in fact the Fe—O and O—O

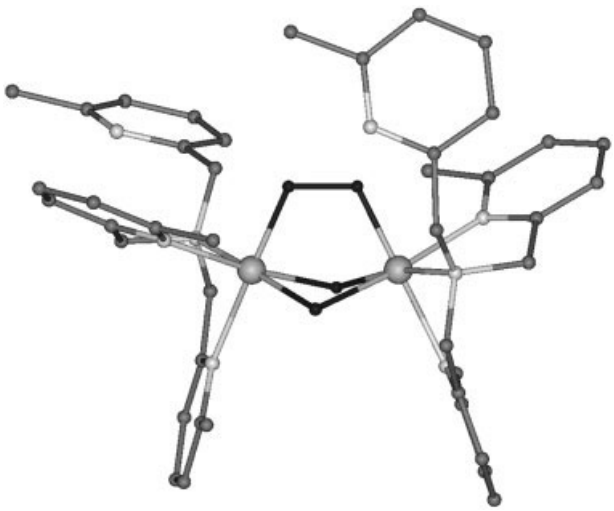

FIGURE 5. Calculated structure of Compound **3**, formed from **1** by addition of O_2 to create a peroxide bridge.

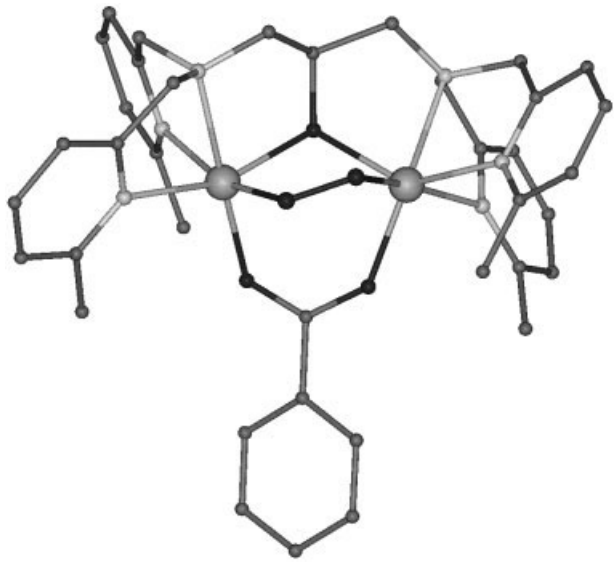

FIGURE 6. Calculated structure of Compound **4**, formed from **2** by addition of O_2 to create a peroxide bridge.

distances and charge distributions are also similar in the two compounds. The calculated low frequency Fe—O stretches for **4** were found to lie at 377 cm^{-1} and 437 cm^{-1}. The O—O stretch was found to lie at 948 cm^{-1}, and the mode is a nearly pure O—O stretch. Another high frequency mode at 917 cm^{-1} was found to arise primarily from the motion of the single bridging oxygen labeled O1 in Figure 2. The BSLS Fe—O stretches lie at 417 and 446 cm^{-1}. As with Compound **3**, the BSLS Fe—O bond lengths are shorter than are the HS. However, the BSLS O—O bond length is slightly shorter than the HS, and the calculated O—O stretching frequency is higher, at 994 cm^{-1}. The frequency of the mode dominated by the single bridging oxygen lies at 893 cm^{-1} in the BSLS calculated spectrum. The assignment of the calculated spectrum differs from the experimental assignment in attributing one of the high frequency modes to motions of the single-bridge oxygen rather than attributing both primarily to the peroxide oxygens.

Conclusions

This study of two diiron(II) complexes finds the DFT optimized molecular geometries in both the HS and BSLS representations to be acceptably accurate. Differences between HS and BSLS geometry variables examined are of about the same magnitude as corresponding differences between the BPW91 and BOP results, and these latter employ the same exchange functional. Overall agreement between HS and BSLS geometries is slightly better in the diiron(II) complexes than in the diiron(III) peroxides that arise from their reactions with O_2, and better than the agreement seen in a previous study of diiron(III) complexes [15]. That superior agreement seems derived from attributes of the peroxide bridges as well as from somewhat greater charge transfer from ligands to the Fe(III) ions compared to the Fe(II).

HS and BSLS calculations result in different spin densities and different polarization of the spin densities on the bridging oxygens. With the singly bridging oxygens, the HS and BSLS bond lengths and Fe—O—Fe angle differ by no more than they do with two different density functionals. However, in the peroxide bridge, HS and BSLS Fe—O lengths differ by as much as 0.2 Å. In Compound **3** the Fe—O—O—Fe dihedral is nearly 0° in both HS and BSLS calculations, but in **4** the difference is 15°. Crystal structures of neither are available, so which is more accurate is unknown, but previous calculations on a complex with considerable buckling in a peroxide bridge found the BSLS dihedral to be accurate [15].

The differences seen in the HS and BSLS charge density distributions are to be noted as well in the calculated harmonic frequencies associated with the atoms of the peroxide bridges. Here, the rather large errors, as much as 20% in the low-frequency vibrations, make it difficult to assess which approach yields more accurate spectra. However, both affirm the experimental spectral assignments, with the single exception that in one band of Compound **4** the analysis of the experimental spectrum seems to exaggerate the contribution of a peroxide vibration.

ACKNOWLEDGMENTS

DEB acknowledges the support of the Consejo Nacional de Investigaciones Científicas y Técnicas de la República Argentina.

References

1. Feig, A. L.; Lippard, S. J. Chem Rev 1994, 94, 759.
2. Kurtz, D. M. J Biol Inorg Chem 1997, 2, 159.
3. Stenkamp, R. E. Chem Rev 1994, 94, 715.
4. Liu, X.; Theil, E. C. Acc Chem Res 2005, 38, 167.
5. Bacelo, D. E.; Binning, R. C. Inorg Chem 2006, 45, 10263.
6. Kohn, W.; Sham, L. J. Phys Rev A 1965, 140, 1133.
7. Ziegler, T.; Rauk, A.; Baerends, E. J. Theor Chim Acta 1977, 43, 261.
8. Jones, R. O.; Gunnarsson, O. Rev Mod Phys 1989, 61, 689.
9. Torrent, M.; Musaev, D. G.; Basch, H.; Morokuma, K. J Comput Chem 2002, 23, 59.
10. Torrent, M.; Musaev, D. G.; Morokuma, K. J Phys Chem B 2001, 105, 322.
11. Noodleman, L. J Chem Phys 1981, 74, 5737.
12. Noodleman, L.; Baerends, E. J. J Am Chem Soc 1984, 106, 2316.
13. Baik, M.-H.; Newcomb, M.; Friesner, R. A.; Lippard, S. J Chem Rev 2003, 103, 2385.
14. Noodleman, L.; Lovell, T.; Han, W. G.; Li, J. Chem Rev 2004, 104, 459.
15. Binning, R. C.; Bacelo, D. E. J Comput Chem 2008, 29, 716.
16. Siegbahn, P. E. M. Inorg Chem 1999, 38, 2880.
17. Du Bois, J.; Mizoguchi, T. J.; Lippard, S. J Coord Chem Rev 2000, 200, 443.
18. Tshuva, Y.; Lippard, S. J Chem Rev 2004, 104, 987.
19. MacMurdo, V. L.; Zheng, H.; Que, L. Inorg Chem 2000, 39, 2254.

20. Hayashi, Y.; Kayatani, T.; Sugimoto, H.; Suzuki, M.; Inomata, K.; Uehara, A.; Mizutani, Y.; Kitagawa, T.; Maeda, Y. J Am Chem Soc 1995, 117, 11220.
21. O'Connor, C. J Prog Inorg Chem 1982, 29, 203.
22. Becke, A. D. Phys Rev A 1988, 38, 3098.
23. Perdew, J. P.; Burke, K.; Wang, Y. Phys Rev B 1996, 54, 16533.
24. Tsuneda, T.; Suzumura, T.; Hirao, K. J Chem Phys 1999, 110, 10664.
25. Delley, B. J Chem Phys 1990, 92, 508.
26. Delley, B. J Chem Phys 2000, 113, 7756.
27. Ghosh, A.; Taylor, P. R. Curr Opin Chem Biol 2003, 7, 113.
28. Ghosh, A. J Biol Inorg Chem 2006, 11, 712.